Pattern formation of flames in radial microchannels with lean methane-air mixtures

Sudarshan Kumar,[1] Kaoru Maruta,[1] and S. Minaev[2]
[1]*Institute of Fluid Science, Tohoku University, 2-1-1 Katahira, Aoba-ku, Sendai, Japan*
[2]*Institute of Theoretical and Applied Mechanics, SB-RAS Novosibirsk, Russia*
(Received 18 January 2006; revised manuscript received 8 September 2006; published 16 January 2007)

Premixed methane-air mixture is introduced at the center of two parallel circular quartz plates separated by a millimeter scale distance ($\leqslant$5 mm). Two plates are heated with an external heater to create a positive temperature gradient condition along the flow direction. The combustion characteristics of lean methane-air mixtures are investigated at ϕ=0.67 and ϕ=0.85 in the laminar flow regime (Re$\sim$500–1800). Contrary to the general perception of a stable premixed flame front at a radial location, a large variety of unstable and dynamic flame front patterns are observed at ϕ=0.67. At ϕ=0.85, stable flame propagation mode dominated the regime diagram and unstable flame propagation modes are observed under limited conditions. In these unstable flame propagation modes, single and multiple flame fronts rotate around the center at a rate of 15–50 Hz.

DOI: 10.1103/PhysRevE.75.016208 PACS number(s): 82.40.Bj, 82.40.Ck, 47.54.−r

I. INTRODUCTION

Rotating wave patterns are widely observed in a variety of natural situations, such as propagation of electric pulses in cardiac muscles [1] and chemical reaction in liquid phase (B-Z reaction media) [2], gaseous premixed [3–7], nonpremixed [8], and solid phase [9] combustion systems. In combustion, many references are available to the phenomena of wave propagation, pattern formation and flame front instabilities. The understanding of these phenomena becomes more complex as the process is governed by nonlinear coupling of fluid dynamics, chemical reaction, and heat and mass transfer properties of fuel and oxidizer. Different types of flame instabilities are reported in literatures [10,11]; hydrodynamic, buoyancy driven, thermal-diffusive, and viscous fingering. A prodigious amount of work has been reported by different researchers in the fields of cellular flames [3], spiral flames [4–8], and fingering instability [12,13] in premixed and nonpremixed [8] combustion to model and explain these phenomena.

The present work concerns with the experimental observation of the flame instabilities and formation of various rotating flame patterns in radial microchannels. The interest in microscale combustion devices arises due to major advantages associated with these small-scale systems. Some of these advantages include higher heat and mass transfer coefficients, orders of magnitude higher energy densities of hydrocarbon fuels compared to that of electrochemical batteries ($\sim$20–50 times higher) and abatement of pollutant emissions from these systems due to lower operating temperatures [14–16]. The increased heat loss due to large surface area-volume ratio adversely affects the combustion stability limits in these devices. To obtain stable combustion, thermal management, for instance, heat recirculation is a key factor for efficient operation of these small scale devices [16–18]. In this technique, combustor walls in the downstream are kept at high temperature due to heat of combustion and incoming mixture is preheated by those hot walls. Wall thickness and thermal conductivity of solid walls play an important role, which determine the heat recirculation performance of the system configuration. Detailed theoretical analysis and numerical studies on the effect of these parameters on heat recirculation have been reported by Ronney [16] and Norton and Vlachos [18].

Maruta *et al.* [15] have studied the flame propagation characteristics of premixed methane-air mixtures in a 2 mm diameter straight quartz tube with a positive temperature gradient along the flow direction as shown in Figs. 1(a) and 1(b). This is a simple one-dimensional configuration to study flame propagation characteristics in microchannels which resembles to a system with heat recirculation through channel walls. Steady state wall temperature gradient was given to the channel walls to simplify the target model. This strategy is employed to avoid transient thermal coupling between gas and solid phases. This simplification can be justified if the heat capacity of the solid phase is much larger (thermally thick) than that of gas phase which is often true for microdevices having microchannels in them. The theoretical study shows the existence of a steady premixed flame at high and extremely low mixture velocities as shown by solid thick lines in Fig. 1(c). Various unstable flame propagation modes are observed experimentally at intermediate mixture velocities as predicted [15,19] and these modes are denoted by dotted lines in Fig. 1(c). These unstable propagation modes are classified as (a) pulsating flame, (b) flames with repetitive extinction and ignition (FREI), and (c) a combination of pulsating and FREI modes. The appearance of these unstable modes is attributed to the existence of flame bifurcation points and excitation of flame oscillations at these intermediate mixture velocity conditions [15]. The linear stability analysis also supports the existence of different stable and unstable propagation modes which are observed experimentally at intermediate mixture velocities [19]. The nonlinear flame analysis of this configuration in the unstable zone shows that a small perturbation grows to full oscillations. The trajectory and amplitude of these oscillations settles to a constant value and the oscillation pattern exhibits characteristics pertinent to the FREI phenomena [20].

The observation of various unsteady and pulsating modes in a straight channel [15] motivated the authors to investigate and understand these flame instabilities in a two-dimensional (2D) configuration, such as radial channels. Hence, the experimental observations of dynamic, unsteady, and rotating

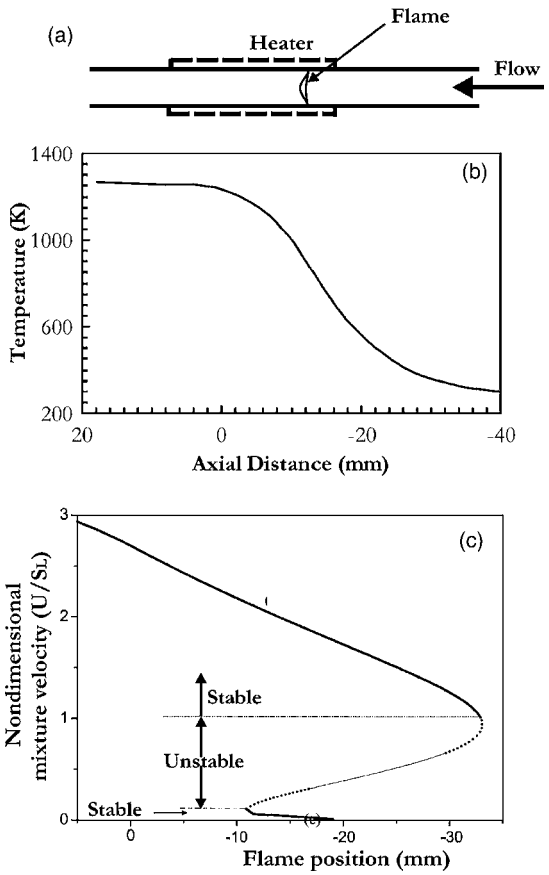

FIG. 1. Flame propagation in a 2 mm diameter 1D straight quartz tube. (a) Schematic of the straight channel (b) wall temperature profile (c) variation of flame front location with mixture velocities [15].

flame propagation modes in radial microchannels with steady state positive temperature gradient for lean methane-air mixtures are reported in this work. Rich methane-air mixtures subjected to these conditions results in the formation of quasisteady spiral and radial flame propagation modes [6]. In a real practical application, fuel-air mixture is supplied to a combustion chamber configuration such as disk-type micro gas turbine (MIT micro gas turbine) [21], which is similar to the present configuration.

The structure of the present paper is as follows. The details of present experimental setup are described in the Sec. II. In Sec. III, the preliminary experimental observations are discussed. This is followed by regime diagrams for different flame propagation modes at $\phi=0.67$ and 0.85. The propagation characteristics of these flame modes are discussed in the following sections. A brief discussion on the observation of these flame propagation modes and summary of the present work are presented in the subsequent sections.

II. EXPERIMENTAL SETUP

The scheme of the experimental setup is shown in Fig. 2. Two quartz plates are maintained parallel to each other within an accuracy of ±0.1° with the help of a level indicator. To simulate the heat recirculation process, which has a positive temperature gradient along the flow direction, both the plates are heated with a sintered metal burner. This helps to create a positive temperature gradient conditions in the radial direction, when mixture is introduced at the center through a 4 mm diameter mixture delivery tube. The temperature profiles along the inner side of the bottom and top plates are measured in advance by using airflow with a 300 μm size K-type thermocouple. A cooling arrangement is made in the mixture delivery tube to maintain the upstream temperature of the incoming mixture at 300 K. Methane gas with 99.99% purity is used as fuel. Electric mass flow controllers are used to precisely monitor the mass flow rates of methane and air within an accuracy of ±1%.

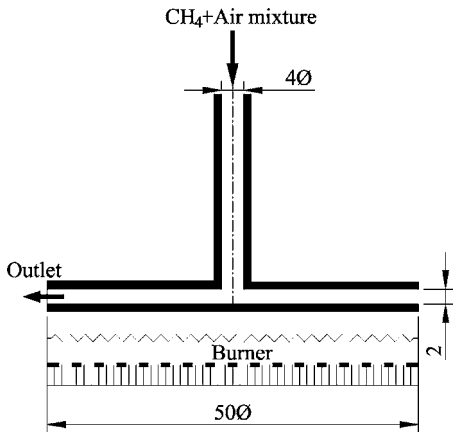

FIG. 2. Experimental setup.

The preliminary observations are carried out with a normal CCD video camera. Due to the unsteady nature of the combustion process, normal movie recording is also carried out with the help of a high speed video camera "FASTCAM-NEO Photron." High speed video recordings are carried out from an angular position of approximately 30° angle sideways because the presence of vertical mixture delivery tube restricts the top view of quartz plates. The picture resolution is 512×512 pixels over a range of the image capturing speeds varying from 30 Hz to 20 000 Hz. Flame images are recorded at a rate of 500 and 1000 frames per second with 1/1000 s 1/2000 s shutter speed respectively. During each run, 2048 frames are recorded and the images are further analyzed with an image processing software PFV-ver.2.2.2.1.

The background flame of the sintered metal burner imparts some noise for direct recording and results in poor visualization of the propagating flame fronts. Therefore, the heating burner had been switched off while carrying out the high speed video recording to present better quality pictures of the observed flame patterns. Flame pattern remains unaffected for approximately 800–2000 ms and the frames presented here are taken within the first 100 ms after the heating burner had been switched off.

III. EXPERIMENTAL RESULTS

A. Wall temperature profile characteristics

The wall temperature profiles on the inner side of the top and bottom quartz plates are measured in advance to exam-

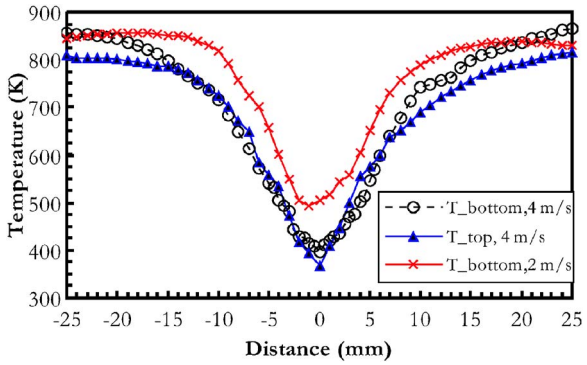

FIG. 3. (Color online) Measured temperature profile of the top plate and bottom plate at different flow velocities.

ine the effects of flow on them. The mixture supply near the center of the plates cools the plates at the center and creates a positive temperature gradient in the flow direction. Figure 3 shows the measured temperature profiles on the inner side of the top and bottom plates for an airflow rate, $Q=3$ SLM (standard liters per minute), (mixture velocity through delivery tube, $U_\infty \sim 4$ m/s) through the delivery tube. The top plate gets heated due to convection and radiation from the bottom plate. In particular, the role of convectional heat transfer decreases in the radial direction due to linear decrease in the Reynolds number because $\mathrm{Nu} \sim \mathrm{Re}^{1/2}$ and $\mathrm{Re} = \rho d^2 U_\infty / 8\mu r$, $\mathrm{Re} \sim r^{-1}$ (where Nu is the Nusselt number, Re is the Reynolds number, and d is the diameter of the mixture delivery tube). Similarly, the role of radiation can also be approximated, which is observed to be significant due to high emissivity of quartz glass ($\varepsilon=0.94-0.96$). Therefore, the measured temperature distribution of both the plates is similar with a slightly lower temperature ($\sim 20-50$ K) of the top plate. This was also confirmed with the wall temperature measurements using an infrared thermoviewer. To quantify the effects of mixture velocity on the temperature profile, wall temperature measurements were carried out over a range of velocities varying from 2–7 m/s ($Q \sim 1.5-5.25$ SLM) and the bottom plate temperature measurements for a velocity of 2 m/s are shown in Fig. 3. It has been observed that with the decrease in the airflow velocity, the overall temperature profile shrinks, when compared to the temperature profile at 4 m/s. Similarly, an increase in the velocity leads to the widening of the temperature profile. To summarize, the variation in the peak temperature is observed to be less than ±40 K over a range of mixture velocities for the present experiments (2–7 m/s, $Q \sim 1.5-5.25$ SLM).

B. Preliminary investigations

Parametric studies are carried out to distinguish the different flame propagation modes observed in the present experiments. Mixture equivalence ratio, plate separation distance, and mixture velocity are important parameters which affect the formation of these rotating flame patterns. The typical mixture velocity through mixture delivery tube is varied in the range of 2–7 m/s ($\mathrm{Re} \sim 500-1800$, $Q = 1.5-5.25$ SLM). The present results are limited to 7 m/s

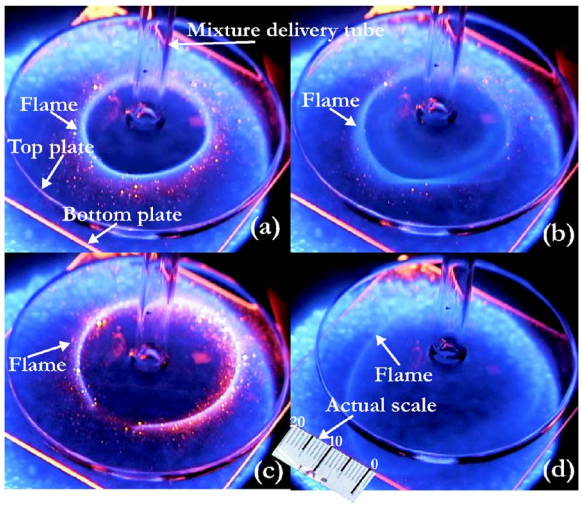

FIG. 4. (Color online) Preliminary observations on various flame propagation modes with a digital video camera. (a) *A*-stable (b) *B*-regime unstable propagation mode (c) *A*-broken (d) *C*-Regime propagation mode.

mixture velocity because the flow is expected to become turbulent at ~9 m/s ($\mathrm{Re} \sim 2300$, $Q=6.75$ SLM) in the mixture delivery tube and experimental investigations did not show any significant change in the observed flame behavior for 7–9 m/s ($Q=5.25-6.75$ SLM) velocity range. Fuel supply is initiated after steady state plate temperatures are attained along with the continued air supply through delivery tube. The distance between two quartz plates is maintained at 5 mm at the start of the experiment. The plate separation distance is varied from 5 mm to 0.25 mm in 0.25 mm steps with the help of a micrometer traverse (0.05 mm resolution). The different flame propagation modes are categorized using following schemes.

(1) Propagation modes with stable behaviors are assigned to group *A* (*A*-stable, *A*-broken, *A*-travel are different names assigned to distinguish these modes).

(2) Propagation modes with unstable behaviors are assigned to group *B* (*B*-Pelton, *B*-triple, *B*-symmetrical, *B*-unsymmetrical, *B*-radial, and *B*-spiral are different name assigned to distinguish these modes).

(3) The flames stabilized near the up and downstream ends of the channel are observed and these are equated to flame flashback and flame blowout at low and high velocities, respectively. These limits are classified into regimes *C* and *D* and a brief description is given in the following sections.

Preliminary observations are carried out with a CCD video camera as shown in Fig. 4. Various stable and unstable flame propagation modes are observed over a range of operating conditions. In the combustion regime *A*-stable, a stable flame front is located at a radial location as shown in Fig. 4(a). The radial location of flame front is a function of mixture velocity, equivalence ratio and plate separation distance. Figure 4(b) shows the observation of an unstable flame propagation mode. Details on these unstable flame propagation modes are presented in the following sections.

Figure 4(c) shows the *A*-broken combustion mode. This propagation mode generally appears for very small plate

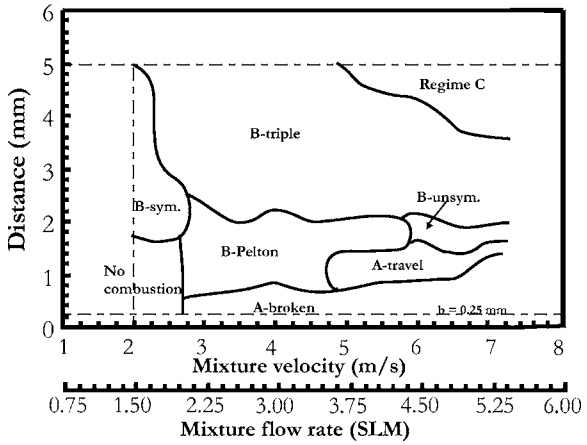

FIG. 5. Regime diagram for various flame propagation modes at $\phi=0.67$ for methane-air mixtures with mixture flow rate varying from 1.5–5.25 SLM ($U\sim2$–7 m/s) and $b\sim0.25$–5.0 nm. The width of the radial channel is changed from 0.25–5.0 mm in 0.25 mm steps. Flame quenching occurred for channel widths smaller than 0.25 mm and not addressed in the figure.

separation distances, where the flame quenches locally at one point in the domain. Figure 4(d) shows the combustion regime *C*, which is observed at high velocity and large plate separation distance. In this regime, a stable flame front with an unsymmetrical flame shape is located near the outer edges of the circular plates. Regime *D* is generally observed at low mixture velocities (<2 m/s) and higher equivalence ratios. In this mode, a stable flame exists at the exit of the mixture delivery tube and resembles to a flame stabilized at the outlet of a straight tube.

C. Regime diagrams at different mixture equivalence ratios

Figures 5 and 6 show the detailed combustion regime diagrams for lean methane-air mixtures at $\phi=0.67$ and 0.85, respectively. These figures show the strong dependence of plate separation distance and mixture velocity for different stable and unstable flame propagation modes. Two equivalence ratios of $\phi=0.67$ and 0.85 are chosen on the lean side for methane-air mixtures because remarkably different flame propagation characteristics are observed at these equivalence ratios. For instance, at $\phi=0.85$ or higher, *A*-stable flame propagation mode dominates the regime diagram compared to leaner mixture (for instance $\phi=0.67$ for present case) conditions at which many unstable and rotating flame propagation modes are observed.

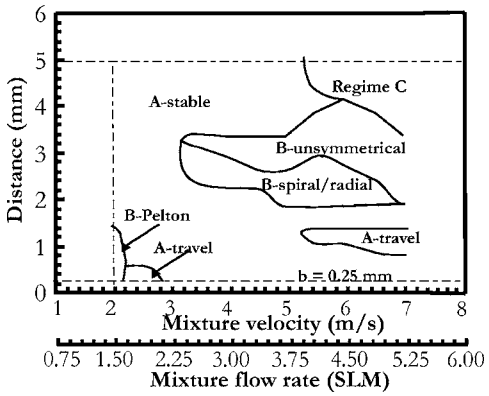

FIG. 6. Regime diagram for various flame propagation modes at $\phi=0.85$ for methane-air mixtures with mixture flow rate varying from 1.5–5.25 SLM ($U\sim2$–7 m/s) and $b\sim0.25$–5.0 mm. The width of the radial channel is changed from 0.25–5.0 mm in 0.25 mm steps. Flame quenching occurred for channel widths smaller than 0.25 mm and not addressed in the figure.

The regime diagrams for rich methane-air mixtures present a similar behavior to that of $\phi=0.85$ [6]. At $\phi=0.67$, various unstable flame propagation modes like *A*-travel, *B*-triple, *B*-Pelton, *B*-symmetrical, and *B*-unsymmetrical dominate most of the regime diagram. The characteristics of these notable flame patterns which dominate the regime diagrams are discussed further in the following paragraphs. The absence of stable flame propagation mode (A-stable) at $\phi=0.67$ (Fig. 5) hints at the difficulty in achieving stable combustion at small scales due to restricted stability limits on the leaner side. Contrary to the existence of these unstable flame propagation modes, at $\phi=0.85$, the stable combustion limits are much wider. The complete quenching of the flame was observed for very small channel gaps, $b<0.25$ mm. For a channel gap of approximately 0.25 mm, a partially quenched flame (denoted by *A*-broken mode) was observed. Further decrease in the channel width led to complete flame quenching in the radial channel. Since the experimental observations are carried out for every 0.25 mm channel widths (in 0.25 mm steps, varying from 0.25 mm to 5.0 mm), complete flame quenching which occurred between 0–0.25 mm channel width is not reflected to the figures for these experiments. The quenching distances for methane-air mixtures in heated radial channels for $\phi=0.67$ and 0.85 are expected to be different.

D. Various stable and unstable flame propagation modes

1. A-stable propagation mode

Figure 6 shows that a stable flame front at a radial location [*A*-stable mode, shown in Fig. 4(a)] exists over a wide range of operating conditions. However, this stable flame propagation mode disappears at lower mixture equivalence ratios (at $\phi=0.67$). The radial location of this flame front is a function of the mixture velocity and the plate separation distance. Mixture equivalence ratio also affects the radial position of this stable flame front through the change in burning velocity.

2. A-travel propagation mode

Figures 7 and 8 show the high speed photographs for the *A*-travel flame propagation mode (see movie clips "a-travel1.avi" and "A-travel2.avi" in Ref. [22]). Figure 7 shows the flame front positions after 1 ms time intervals. White lines are drawn to indicate the position of top plate, plate center, and mixture delivery tube. Two sets of arrows are drawn in the figure to track the flame front movements of fronts 1 and 4. These pictures are recorded at $\phi=0.85$, U_∞

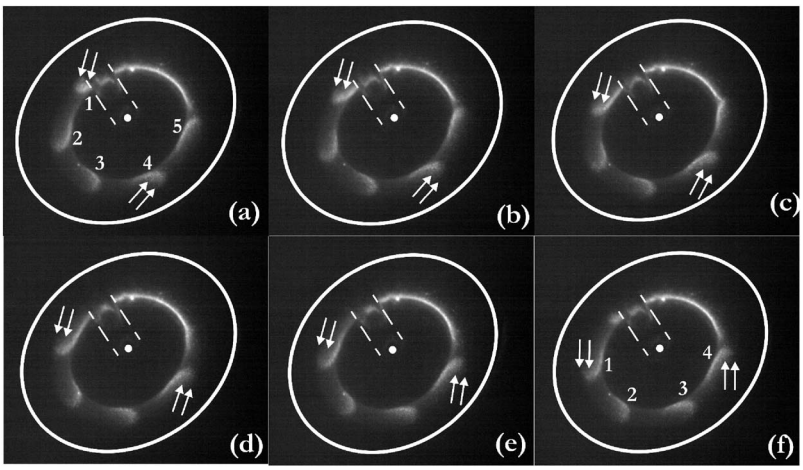

FIG. 7. A-travel flame propagation mode. These images are recorded at 1000 frames per second and 1/2000 s shutter speed and each image shows flame front position after 1 ms time intervals. These frames are recorded at $\phi=0.85$, $U_\infty=2.5$ m/s ($Q=1.8$ SLM), and $b=0.25\pm0.1$ mm.

$=2.5$ m/s ($Q=1.88$ SLM) and plate separation distance, $b=0.25\pm0.1$ mm. In this propagation mode, a stable flame front coexists with traveling flame fronts over a certain angular domain. A small propagating flame front breaks from this stable flame and continues to propagate through the domain in a circular motion and attaches to the stable flame front on the other side. Five small flame fronts denoted as 1, 2, 3, 4, and 5 coexist in the experimental domain simultaneously along with the stable, main flame front. These small flame fronts are nearly half-circular in shape with a slightly longer tail on inner side. Figures 7(a)–7(c) shows the merger of the small flame front 5 with the main stable flame. After the completion of merger, the main stable flame attempts to regain its earlier shape and size. However in the mean time, the next approaching flame front (flame front 4) attempts to merge with the main flame. In a similar fashion, these small flame fronts develop and then separate from the other side of the main stable flame front [flame front 1 in Figs. 7(a)–7(d)] and this phenomenon continues to repeat at a certain rate.

Another interesting phenomena with a similar feature was observed at $\phi=0.67$, $U_\infty=5$ m/s ($Q=3.75$ SLM), and $b=1.5$ mm, as shown in Fig. 8. This figure shows the flame front positions after 2 ms time intervals. White lines are drawn to indicate the top plate position, center, and mixture delivery tube. A set of white arrows is drawn to indicate the position of flame fronts. Figure 8(a) shows that two stable flame fronts exist opposite to each other in the experimental domain and traveling flame fronts emanate from these stable flame fronts. The existence of two stable flame fronts opposite to each other shows that the appearance of traveling flame modes is independent of the plate alignment to a certain extent and perhaps this mode appears as an intermediate state between two stable and unstable flame propagation modes. Figures 8(b)–8(e) shows the further development of these traveling flame fronts followed by a separation of the traveling flame fronts from the main flame front and reattachment with the other stable flame front. This cycle continues to repeat in this propagation mode. Since the small flame fronts break from the main flames and continue to travel in the domain, this mode is named as *A*-travel flame propagation mode.

3. A-broken propagation mode

A-broken flame propagation mode was shown in Fig. 4(c). This picture is recorded at $\phi=0.85$, $U_\infty=3$ m/s ($Q=2.25$ SLM), and $b\leqslant0.25$ mm. This mode is generally observed to exist at a very small plate separation distance, where a stable flame front along with a local flame hole on the flame front exists in the domain. At larger channel widths ($\sim1-2$ mm), various unstable flame propagation modes appear in the combustion zone, where traveling and rotating flame fronts are observed (such as *B*-Pelton and *A*-travel at

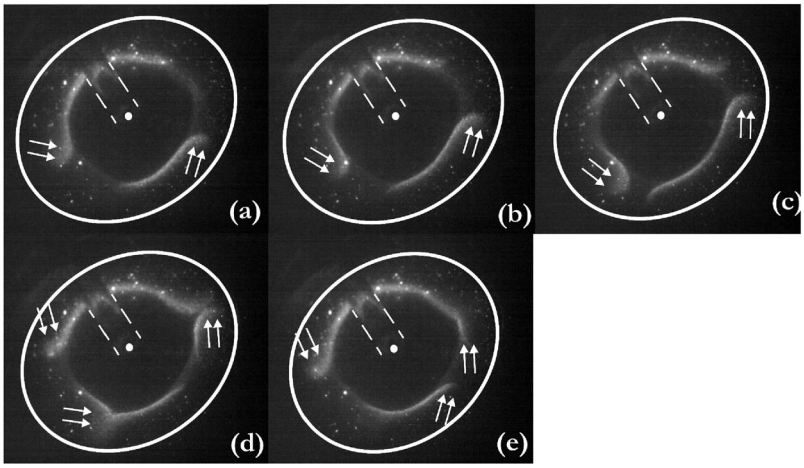

FIG. 8. *A*-travel flame propagation mode. These images are recorded at 1000 frames per second and 1/2000 s shutter speed and each frame shows the flame front position after 2 ms time intervals. These frames are recorded at $\phi=0.67$, $U_\infty=5$ m/s ($Q=3.75$ SLM), and $b=1.5$ mm.

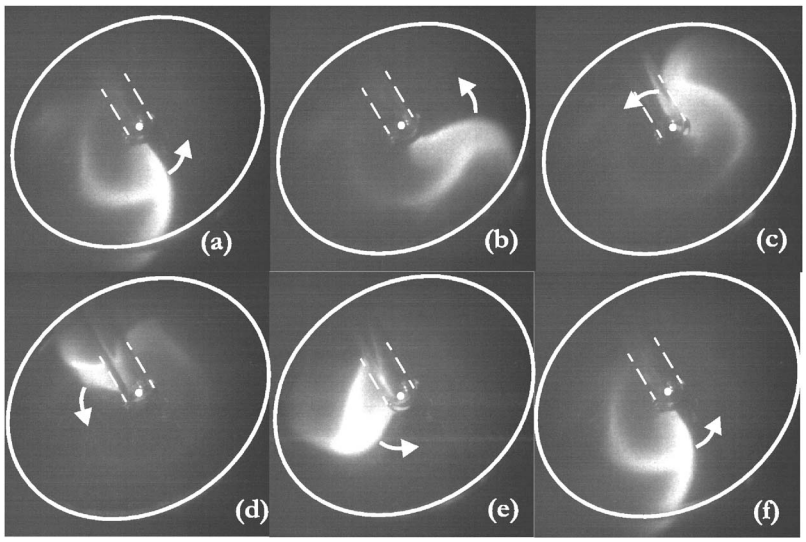

FIG. 9. *B*-triple flame propagation mode. These images are recorded at 500 frames per second and 1/1000 s shutter speed and each image shows the flame front position after 10 ms time intervals. These images are recorded at $\phi=0.67$, $U_\infty=4$ m/s ($Q=3$ SLM), and $b=3$ mm.

$\phi=0.67$). These flame instabilities (unstable flame propagation modes, such as *A*-travel and *B*-Pelton) develop and grow on the flame front due to decrease in the channel width, and an increase in the average flow velocity (due to decrease in channel width) leads to a local flame blowout at the weakest point on the flame front and this creates a local extinction spot on the flame front. Another possibility for the growth of these instabilities and formation of the flame hole is due to the existence of a small asymmetry in angular direction, despite the fact that the plates are heated with a circular cross-section sintered metal burner. Near the extinction limit, these asymmetries and nonlinear growth of small perturbations plays a significant role in the formation of a flame hole. Due to adverse conditions of increased mixture velocity, the mixture reignition becomes difficult and therefore, two flame edges are created on either side and the flame propagation in this mode is perhaps governed by the edge flame propagation mechanism [23]. The extinction spot easily propagates in the angular direction. Bayliss *et al.* [24] also report the formation of similar local flame extinction spots with single and multiple flame kinks in a circular rotating cylindrical burner for various fuel-air mixtures.

4. B-triple propagation mode

In the *B*-triple combustion mode, a long curved flame front extending from the center to the outer edge of the quartz plate followed by a long tail at the center of the curved flame front is observed as shown in Fig. 9. A movie clip, for this flame propagation mode is shown in "*B*-triple.avi" in Ref. [22]. This flame front shape is superficially similar to that of a triple flame with a curved front and long tail in the middle of the propagating flame front [25]. Therefore, this flame propagation mode is named as *B*-triple flame propagation mode. The physics of the *B*-triple flame propagation mode observed in the present experiments is expected to be different from that of a conventional triple flame [25].

The flame front follows a cyclic motion around the centre of the plate. To confirm this, a point is selected on the propagating flame front and this point is tracked for approximately ten complete rotations of the flame front. The tracking point follows a near circular trajectory every time which confirms the nearly circular motion of the propagating front. The circular motion of the propagating flame front could be attributed to the symmetrical temperature distribution of the bottom plate. An asymmetrical temperature distribution affects the flame trajectory to a certain extent. The detailed investigations showed that the propagating flame front follows an asymmetrical trajectory depending on the actual nature of the temperature profile [26]. This flame front is observed to rotate both in a clockwise and a counterclockwise direction with nearly equal probabilities. The onset of the rotational direction in this flame propagation mode is not clear at this moment; however, it could be possible that the direction of rotation is triggered through an internal or external disturbance at a particular location, which decides the rotational direction for the flame front. A similar rotational behavior of spiral flames propagating in a tube is observed by Pearlman and Ronney [4] and Pearlman [5]. Each frame in Fig. 9 shows the flame front position after 10 ms time intervals. This flame pattern is observed mostly under lean mixture conditions and large plate separation distance ($\sim$2–4 mm) and over a range of mixture flow rates as shown in the Fig. 5. The typical rotational speed of this flame front is $\sim$18 Hz. However, the flame rotational speed is observed to be a strong function of plate temperatures and mixture velocities. Further experiments are being carried out to investigate these issues and characterize the rotational behavior and propagation mechanism of the *B*-triple flame propagation mode.

5. B-Pelton propagation mode

Figure 10 shows the flame behavior for regime *B*-Pelton (see a movie clip "B_pelton.avi" in Ref. [22]). Each frame in the figure shows the flame front position after 4 ms time intervals. The typical semicircular shape of the flame front coupled with the rotational motion in this regime makes it to resemble a classical power generating Pelton wheel. In this regime, one, two or three unstable flame fronts, nearly half circular in shape are observed, which revolve around the center of the plates in a cyclic motion [26]. These multiple

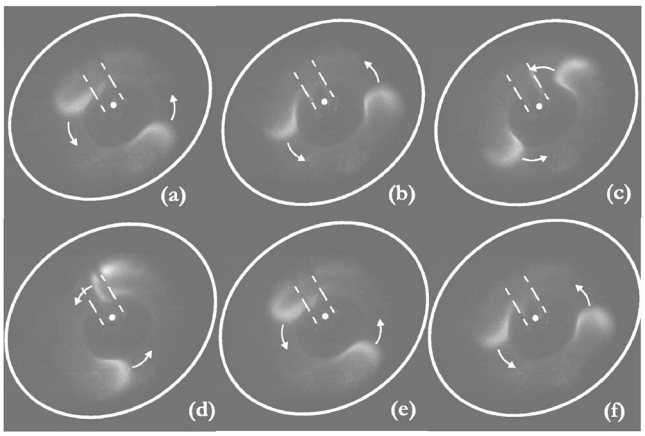

FIG. 10. *B*-Pelton flame propagation mode. These images are recorded at 500 frames per second and 1/1000 s shutter speed and each image shows the flame front position after 4 ms time intervals. These images are recorded at ϕ=0.67, U_∞=4 m/s (Q=3 SLM), and b=1.5 mm.

rotating flame fronts are separated by an equal angular distance (180° angle for present mode with two flames as shown in Fig. 10). Compared to *B*-triple flame propagation mode, for *B*-Pelton propagation mode the flame front is located at a particular radial location depending on the mixture velocity and mixture equivalence ratio. The flame fronts rotate around the center of the plates at this radial position unlike the regime *B*-triple where the flame front is extended till the center of the quartz plate. The typical rotational speed for this flame front is ~30 Hz.

6. B-symmetrical propagation mode

Figure 11 shows the photographs for the flame front propagation in the *B*-symmetrical regime (see a movie clip "B_sym.avi" in Ref. [22]). These images are taken with the heating burner working in the background because the flame

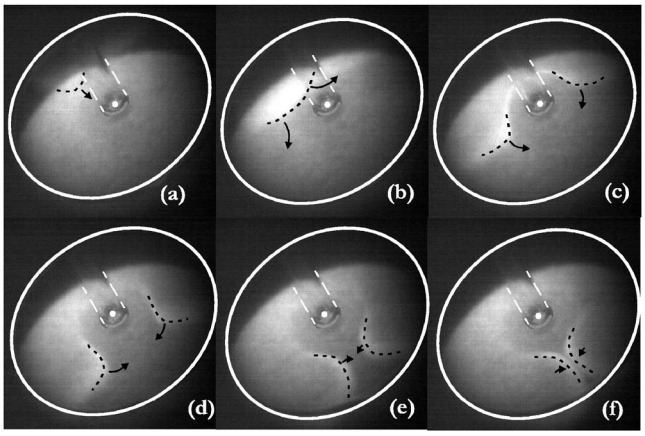

FIG. 11. *B*-symmetrical flame propagation mode. These images are recorded at 500 frames per second and 1/1000 s shutter speed. (a)–(e) shows the flame front position after 4 ms time intervals and (f) shows flame front position after 2 ms time interval. These images are recorded at ϕ=0.67, U_∞=2 m/s (Q=1.5 SLM), and b =3.0 mm.

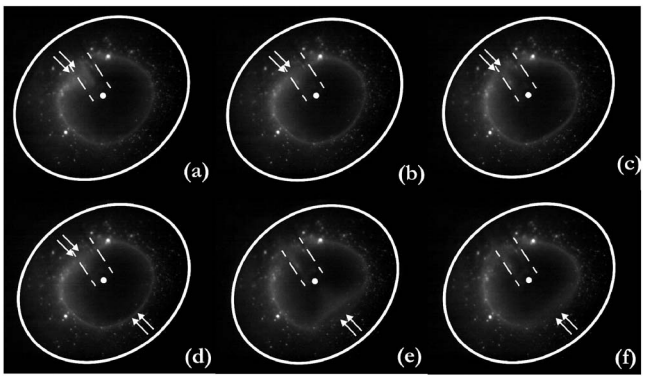

FIG. 12. *B*-unsymmetrical flame propagation mode. These images are recorded at 1000 frames per second and 1/2000 s shutter speed. Each image shows the flame front position after 4 ms time intervals. These images are recorded at ϕ=085, U_∞=4.5 m/s (Q =3.38 SLM), and b=3.0 mm.

propagation behavior changed completely after the heating burner had been switched off. Due to this reason, the image quality is slightly inferior compared to other flame propagation modes. Figures 11(a)–11(e) show the propagating flame front position after 4 ms time intervals and Fig. 11(f) shows the flame front positions after 2 ms time intervals. To indicate the exact position of the flame front, black dashed lines are drawn. Arrows show the direction of the flame front propagation. In this regime, a flame front propagation starts from the edge of the quartz plates and then moves towards the center of the plate. Due to high mixture velocity and unfavorable conditions (high mixture velocity and low wall temperature near the center, lower residence time), the flame front splits into two at a certain radial location in the domain. These two flame fronts are almost mirror images to each other and after following a circular path, they reattach on the other side of the plate after completing a rotation of ~180° in ~20 ms. This sequence of flame propagation in the *B*-symmetrical mode is observed to repeat after every 50–80 ms.

7. B-unsymmetrical propagation mode

Figure 12 shows the direct images taken with a high speed camera to reveal the fluctuations in the flame structure during this unstable flame propagation mode (see a movie clip "Bunsym.avi" in Ref. [22]). A mixture velocity of 4.5 m/s (Q=3.38 SLM) at ϕ=0.85 and plate separation distance of 3 mm are maintained to observe this flame propagation mode. This mode generally appears during transition from one *A*-stable regime to another *A*-stable regime when plate separation distance is reduced from 4 mm to 1 mm. A random instability is generated at a point on the stable flame front which grows with time and moves radially inwards and outwards. Figures 12(a)–12(f) shows that flame instability grows with time and travels towards the center as indicated by two white arrows. In most situations, the flame front oscillates at a single or multiple locations about its mean radial position as shown in Fig. 12. These fluctuations in the flame front radius are quite random in nature and they grow with

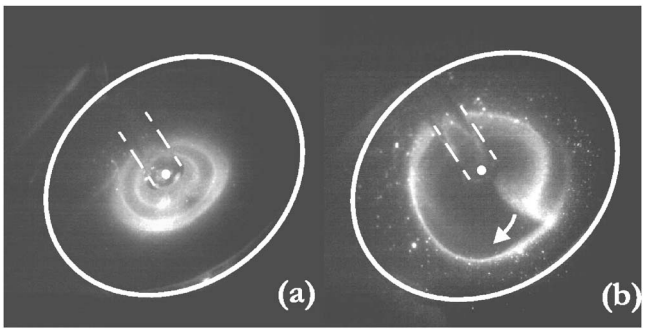

FIG. 13. Radial and spiral flame propagation modes observed at $\phi=0.85$.

time leading to oscillations of the flame front in the radial and angular direction.

8. Radial and spiral flame propagation modes at $\phi=0.85$

Radial and spiral flame propagation modes are observed at $\phi=0.85$ for a range of mixture velocities and plate separation distance, $2 \leqslant b \leqslant 3$ mm. Figure 13 shows the flame front photographs in these propagation modes (see movie clips "*B*2_radial.avi" and "*B*2_spiral.avi" in Ref. [22]). For the radial flame propagation mode (observed at lower mixture velocity), the flame instability moves along the circular flame and develops into a flame kink. This flame kink suddenly ignites the mixture closer to the center and forms a circular ring structure at a smaller radius compared to the original flame location at a larger radius. This is evident from Fig. 13(a) which shows the simultaneous existence of two circular flames at different radial locations. Alternate layers of reactants and combustion products exist at the interface for very small time intervals. Due to high mixture velocity and low residence time near the mixture source, the inner flame starts moving outwards. The original flame front at a larger radius weakens over a period of time due to the unavailability of fresh reactants and finally extinguishes. This whole process described in the preceding lines occurs over a very short time of 8–10 ms. This process repeats after every 30–50 ms. Figure 13(b) shows a so-called spiral flame observed at $\phi=0.85$. In this mode, the flame tip appears to be slightly thickened, which extends towards the center. This is followed by a thin and long tail flame with its length greater than the 2π angle. There exists an interface of fresh mixture reactants and combustion products [6]. This interface is responsible for a long tail flame observed in the present experiments. These engulfed reactants keep burning for a longer time and are responsible for the extension of the flame tail beyond the 2π radial length. The flame rotates continuously around the center and tries to move towards the center to achieve a stable state. However, due to adverse conditions (higher flow velocity and smaller residence time), the flame is pushed away from the center. Hence, the flame continues rotating in this unstableand quasisteady spiral state at a certain frequency. It has been observed that during this state a decrease in mixture velocity results in the appearance of the *A*-stable flame as shown in Fig. 6 (for mixture velocity $\leqslant 3$ m/s).

TABLE I. Summary of the mixture equivalence ratios for various flame propagation modes with different fuel-air mixtures.

Propagation mode	CH_4-Air (Le$\sim$0.95-1.05)	C_3H_8-Air (Le$\sim$1.83)	C_4H_{10}-Air (Le$\sim$2.13)
B-Pelton	0.67	0.55	0.54
B-spiral	0.85–1.33	0.78–0.86	0.74–0.84
B-triple	0.67	Not observed	Not observed
A-Stable	0.80–onwards	0.65–onwards	0.65–onwards

9. Regime C and D

Flames in regime *C* exist near the outlet of the radial microchannel. This mode is generally observed at a large plate separation distance (>4 mm) and a higher mixture velocities (>5 m/s). In this mode, the visibility of the flame front is very low and this mode generally appears near the flame blowout at high mixture velocity and therefore assigned into regime *C* to distinguish the high mixture velocity limit.

At low mixture velocities (<2 m/s) and higher equivalence ratios, a stable flame is observed at the exit of mixture delivery tube, that is, at the center of the plates. This mode is assigned into regime *D*. The presence of the flame at the mixture delivery tube exit results in the breakdown of positive temperature gradient condition. These flames in regime *C* and *D* can be equated to the blowout and flashback conditions because the flame is located either at the outlet or inlet of the radial microchannel.

10. Effect of Lewis number on various flame propagation modes

Different flame propagation modes described in the preceding sections are observed with a lean methane-air mixtures. Hydrodynamic, buoyancy driven, thermal-diffusive, and viscous fingering are some of the mechanisms known for the growth of flame instabilities in laminar premixed and nonpremixed flames [10,11]. The dependence of the flame pattern formation behavior on the Lewis number (thermodiffusive effect) is investigated by employing various fuel-air mixture combinations such as methane, propane, and butane as fuels and a brief summary is presented in this section.

To examine the effect of the Lewis number (thermaldiffusive effect) on these flame propagation modes, various fuel-air mixtures with methane, propane, and butane fuels are employed. The pattern formation characteristics of different fuel-air mixtures are compared for various unstable flame propagation modes and a summary of these investigations is given in Table I. *B*-Pelton flame propagation mode is observed at $\phi=0.67$ for methane-air mixture compared to propane and butane-air mixtures for which the *B*-Pelton mode was obtained at substantially lower equivalence ratios of $\phi=0.55$ and 0.54, respectively. *B*-spiral flame propagation mode is observed in the range of 0.85–1.33 equivalence ratio for methane-air mixtures. A similar propagation mode of spiral flame is observed in $\phi=0.78-0.86$ and 0.74–0.84 equivalence ratio range for propane and butane-air mixtures, respectively. The spiral flame propagation mode was not observed for rich propane and butane-air mixtures, when

compared to the observations with rich methane-air mixtures [5]. *B*-triple (Fig. 9) is another important flame propagation mode which dominates the regime diagram for methane-air mixtures at $\phi=0.67$. However, this propagation mode with a unique shape, similar to that of triple flame was not observed for propane and butane-air mixtures over a range of equivalence ratios varying from 0.3–2.0. The absence of this *B*-triple flame propagation mode with propane and butane-air mixtures hints at the possibility of the Lewis number playing an important role in determining the flame structure for these rotating flame patterns, because the Lewis number for propane and butane-air mixtures is substantially higher than one ($\sim$1.83 and 2.13, respectively), when compared to the Lewis number of lean methane-air mixtures (Le$\sim$0.95). It is more likely that hydrodynamics plays a role in the formation of these flame patterns due to outward flow through the radial channel which experiences an adverse pressure gradient in the radial microchannel. The Reynolds number decreases linearly in the radial microchannel ($\mathrm{Re}=\rho d^2 U_\infty/8\mu r$, independent of channel width) and it is much smaller when compared to the Reynolds number in the mixture delivery tube. For instance, for a mixture velocity of 7 m/s, the Reynolds number in the mixture delivery tube is $\sim$1800 when compared the flow Reynolds number at the radial channel entry, $\mathrm{Re}_{\mathrm{entry}}\sim 450$ and $\mathrm{Re}_{\mathrm{exit}}\sim 40$. Since the flow is laminar and the Reynolds number further decreases in the radial channel, the transition to turbulence is not expected to play a significant role in the formation of these flame patterns. Flow visualization and flow field measurements are being pursued to determine the flow field structure and examine the possibility of flow field coupling with the rotating flame fronts.

IV. DISCUSSION

The appearance of various flame patterns in radial microchannels arises perhaps due to the existence of the flame bifurcation points and excitation of flame oscillations at intermediate mixture flow, velocities, and channel widths. Various instabilities of a pulsating nature had been observed for flames propagating in straight circular channels with a temperature gradient along the flow direction for intermediate mixture velocities [15,19]. The appearance of these pulsating instabilities had been attributed to the transition of the flame solution from stable to unstable branch at these intermediate conditions [Fig. 1(c)]. The present configuration of a radial channel is an example of a neutral system which is symmetric about the vertical axis. Therefore, the excitation of these instabilities in a 2D configuration of radial channels leads to the rotation of these propagation modes around the center in either direction. The onset of the rotational direction could be either due to a random disturbance present at a particular location or due to an external influence.

The balance between the flame propagation velocity and local flow velocity is the basic governing parameter for the formation of these flame patterns [26]. Flame propagation velocity depends on the mixture equivalence ratio, mixture velocity, wall temperature, and channel width. Therefore, the fuel-air mixture conditions along with the local flow conditions determine the flame behavior and appearance of a particular mode. A small deviation in one of these parameters (such as channel width and mixture velocity or equivalence ratio) acts as a perturbation to the flame solution and depending on the growth of these perturbations, which could either lead to a transition from a steady state flame solution to an unsteady flame behavior or transition from one unsteady flame behavior to another unsteady mode. For instance, a transition from steady state flame propagation mode (*A*-stable mode) to an unstable flame propagation mode such as *B*-unsymmetrical, *B*-spiral, or *B*-radial flame propagation mode at $\phi=0.85$ (Fig. 6). Similarly, a transition from one rotational state to another rotational state is observed at lower equivalence ratios, namely at $\phi=0.67$. For instance, at a mixture velocity of 3 m/s and $\phi=0.67$, various flame propagation behaviors are observed when the channel width is reduced from 5.0 mm to 0.25 mm. The pattern of these propagating flame fronts changes from regime *B*-triple to *B*-Pelton and then finally to regime *A*-broken with the decrease in the channel width. The transition from the *B*-triple to the B-Pelton mode occurs at $\sim$2 mm channel width. A decrease in channel width increases the mean flow velocity in the domain, particularly near the center. Therefore, a flame blowout occurs near the center zone and a transition from *B*-triple (Fig. 9) to *B*-Pelton (Fig. 10) mode is observed, where the flame propagates within the radial channel and it does not extend to the center. A further reduction in the channel width leads to the appearance of *A*-broken mode.

At this moment, the exact mechanisms responsible for the formation and propagation of these flame patterns remain unclear, however, these patterns are observed at moderate flow rates and intermediate channel widths, similar to those of the one-dimensional (1D) unstable flame propagation modes [15]. Further work is being carried out in this direction to propose appropriate propagation mechanisms which could be helpful to explain these experimentally observed rotating flame propagation modes. Numerical studies are also being carried out to further understand the flame behavior in these flame propagation modes.

V. CONCLUSIONS

The present paper reports the pattern formation characteristics of flames in radial microchannels with lean methane-air mixtures. The flame propagation behaviors are experimentally examined at 0.67 and 0.85 equivalence ratios. The fuel-air mixture is subjected to a positive temperature gradient and negative velocity gradient conditions simultaneously. A strong dependence of plate separation distance and mixture velocity is observed for different flame propagation modes. Regime diagrams are plotted with these variables for different equivalence ratios. The present investigations show that stable flame propagation mode dominates the regime diagram for $\phi\geqslant 0.85$ and at $\phi=0.67$, various rotating flame patterns are formed. *B*-triple, *B*-Pelton, *B*-symmetrical, *B*-unsymmetrical, and *A*-travel flame propagation modes dominate the regime diagram for $\phi=0.67$. Most of these

patterns rotate at a certain frequency (~15–50 Hz) around the center of plates. The Lewis number effects are investigated by employing propane and butane-air mixtures along with methane-air mixtures. Various flame propagation modes such as *B*-Pelton and *B*-spiral are observed at different mixture equivalence ratios of these fuel-air mixtures. The *B*-triple flame propagation mode is not observed with propane and butane-air mixtures.

ACKNOWLEDGMENTS

The authors would like to thank S. Maruyama, IFS for having useful, interesting, and thought-provoking discussions while carrying out this work. The authors would also like to thank S. Hasegawa for helping in the experimental setup and giving useful suggestions for conducting the present experiments.

[1] J. M. Davidenko, A. V. Pertsov, R. Salomonsz, W. Baxter, and J. Jalife, Nature (London) **355**, 349 (1992).
[2] A. N. Zaikin and A. M. Zhabotinsky, Nature (London) **225**, 535 (1970).
[3] M. Gorman, M. el-Hamdi, and B. Pearson, Phys. Rev. Lett. **76**, 228 (1996).
[4] H. G. Pearlman and P. D. Ronney, Phys. Fluids **6**, 4009 (1994).
[5] H. G. Pearlman, Combust. Flame **109**, 382 (1997).
[6] Sudarshan Kumar, K. Maruta, S. S. Minaev, and R. Fursenko, Phys. Fluids (to be published).
[7] V. Panfilov, A. Bayliss, and B. J. Matkowsky, Appl. Math. Lett. **16**, 131 (2003).
[8] V. Nayagam and F. A. Williams, Phys. Rev. Lett. **84**, 479 (2000).
[9] A. G. Merzhanov, Combust. Sci. Technol. **98**, 307 (1994).
[10] G. I. Sivashinsky, Annu. Rev. Fluid Mech. **15**, 179 (1983).
[11] F. A. Williams, *Combustion Theory* (Benjamin Cummings, 1985), p. 341.
[12] O. Zik, Z. Olami, and E. Moses, Phys. Rev. Lett. **81**, 3868 (1998).
[13] M. L. Frankel and G. I. Sivashinsky, Phys. Rev. E **52**, 6154 (1995).
[14] A. C. Fernadrz-Pello, Proc. Combust. Inst. **29**, 883 (2002).
[15] K. Maruta, T. Kataoka, N. I. Kim, S. Minaev, and R. Fursenko, Proc. Combust. Inst. **30**, 2429 (2005).
[16] P. D. Ronney, Combust. Flame **135**, 421 (2003).
[17] S. A. Lloyd and F. J. Weinberg, Nature (London) **251**, 47 (1974).
[18] D. G. Norton and D. G. Vlachos, Chem. Eng. Sci. **58**(21), 4871 (2003).
[19] K. Maruta, J. K. Parc, K. C. Oh, T. Fujimori, S. S. Minaev, and R. V. Fursenko, Combust., Explos. Shock Waves **40**, 516 (2004).
[20] K. Maruta, T. Kataoka, S. Minaev and R. Fursenko, Combust. Theory Modell. **11**, 187 (2007).
[21] A. H. Epstein, S. D. Senturia, and G. Anthasuresh, IEEE Transducers '97 Conference (Chicago, IL) 753 (1997).
[22] See EPAPS Document No. E-PLEEE8-75-027701 for video clips showing the formation of different flame propagation modes. For more information on EPAPS see http://www.aip.org/pubservs/epaps.html.
[23] J. B. Liu and P. D. Ronney, Combust. Sci. Technol. **144**, 21–46 (1999).
[24] A. Bayliss and B. J. Matkowsky, Physica D **99**, 276 (1996).
[25] G. R. Ruetsch, L. Vervisch, and A. Linan, Phys. Fluids **7**, 1447 (1995).
[26] Sudarshan Kumar, Kaoru Maruta, and S. S. Minaev, Proc. Combust. Inst. **31**, 3261 (2007).